Chapter 9
MgB_2

9.1 Superconducting Properties

MgB_2 is a new metallic superconductor with a critical temperature of about 39 K that was discovered in 2001. This superconductor has superior properties, such as a critical temperature significantly higher than usual for metallic superconductors and less serious issues of anisotropy and weak links at grain boundaries, which are inevitable in high-temperature superconductors. For these reasons, not only fundamental research on physical properties, but also applied research, has been enthusiastically conducted on this superconductor, and important applications are expected, especially around liquid hydrogen temperature. Thus, wires, including multifilamentary ones, and thin films have been fabricated, and investigations have been intensively carried out on their pinning properties, including the irreversibility field.

This superconductor has a layered crystal structure composed of parallel alternate hexagonal close-packed Mg layers and honeycomb B layers. Hence, the electromagnetic properties show an anisotropy due to the crystal structure, and the coherence length in the a-b plane is longer, resulting in a lower value of the upper critical field for the magnetic field direction along the c-axis normal to the plane, as shown in Fig. 9.1 [1]. Its temperature dependence shows a pronounced upward curvature, which can be seen in the figure. This is caused by the two-gap superconductivity in the π and σ bands in the 2p orbital of boron with different critical temperatures. The anisotropy of the upper critical field is shown in the inset. It can be seen that the anisotropy factor is about 2 at the critical temperature and increases with decreasing temperature. The coherence lengths estimated from the upper critical fields are approximately $\xi_c(0) = 9.6$ nm and $\xi_{ab}(0) = 2.0$ nm. These are considerably longer than those in high-temperature superconductors and hence, flux pinning properties similar to those of the usual metallic superconductors are expected.

Figure 9.2 shows the temperature dependence of various characteristic magnetic fields for a polycrystalline specimen [2]. The values of the thermodynamic critical field H_c below 25 K are estimated from the values of the upper critical field H_{c2}, extrapolated from the high temperature region and the observed lower critical field H_{c1}. Thus, the values of H_{c1} and H_{c2} are values averaged with respect to the

T. Matsushita, *Flux Pinning in Superconductors*,
Springer Series in Solid-State Sciences 178,
DOI 10.1007/978-3-642-45312-0_9, © Springer-Verlag Berlin Heidelberg 2014

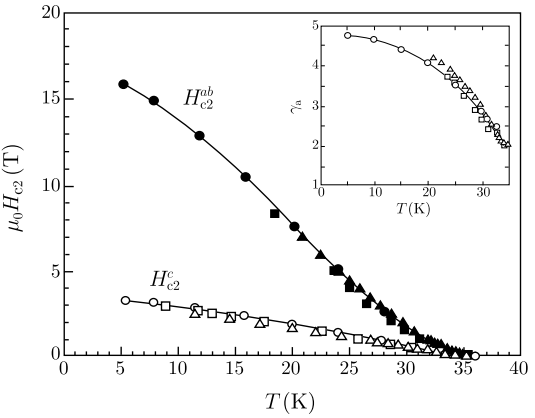

Fig. 9.1 Temperature dependence of upper critical field of MgB_2 single crystal [1]. *Insert* shows the anisotropy of the upper critical field, $\gamma_a = H_{c2}^{ab}/H_{c2}^{c}$

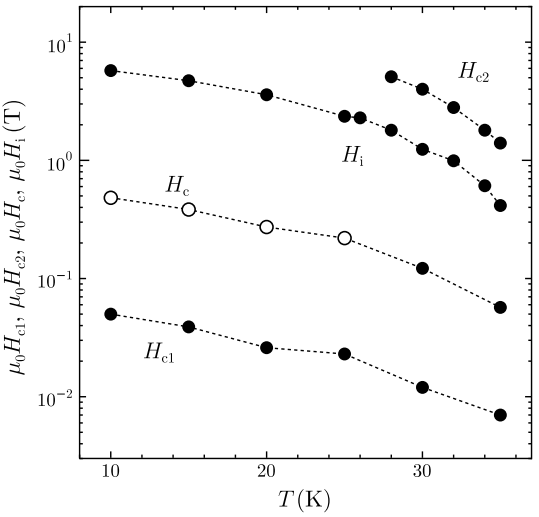

Fig. 9.2 Various critical fields and irreversibility field in MgB_2 polycrystalline specimen [2]. The values of the thermodynamic critical field below 25 K (*open circles*) are estimated using extrapolated values of the upper critical field to the low temperature region

anisotropy. The value of H_c at 10 K is about 0.5 T and is similar to that of Nb_3Sn at 4.2 K. The Ginzburg-Landau parameter, κ, shown in Fig. 9.3 is about 20, and it is independent of the temperature [2]. The coherence length in polycrystalline bulk specimens, wires, or thin films can be shortened, resulting in a significant enhancement of the upper critical field from the values in single crystals, by choosing a suitable annealing temperature or by addition of carbon atoms. As can be seen from Fig. 9.2, the irreversibility field is remarkably lower than the upper critical field in MgB_2 superconductor, although the difference is much smaller than in high-temperature superconductors. Hence, MgB_2 has an irreversible property intermediate between those of metallic and high-temperature superconductors. The main differences from metallic superconductors are higher temperatures for applications and lower critical current densities at the present stage.

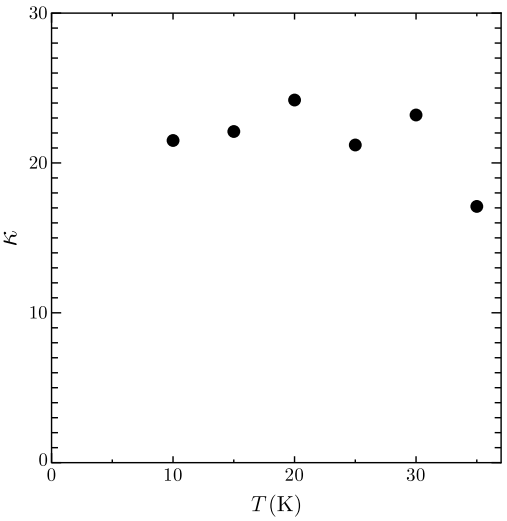

Fig. 9.3 Ginzburg-Landau parameter in MgB_2 polycrystalline specimen [2]

9.2 Critical Current Properties

9.2.1 Wires and Bulk Materials

With respect to the MgB_2 wires being fabricated now, the powder in tube (PIT) process is common, in which a metallic sheath such as iron is packed with powders and then is drawn. There are two methods: one is the *in situ* method, in which mixed powders of magnesium and boron or their compounds are used, with the heat-treatment for the reaction taking place after the drawing, and the other is the *ex situ* method, in which reacted MgB_2 powders are used. The *in situ* wires usually have superior critical current density (J_c) in high magnetic fields.

MgB_2 superconductor in wires is usually polycrystalline, and it is considered that there are no issues of weak links in grain boundaries to influence the transport properties as with metallic superconductors. The critical current density in wires is fairly low, however, in spite of the high condensation energy density, as will be shown later. The reason for the low critical current density can be found in the low density of MgB_2 phase, which is caused by the low packing density of powders and also by the reduction in volume as a result of the chemical reaction in the *in situ* fabrication process. Nucleation of MgO grains or thin MgO layers at grain boundaries is also a dominant factor in low critical current densities. The grain connectivity is evaluated from the normal state resistivity based on the Rowell model [3]. Yamamoto et al. [4] estimated the connectivity K using the cubic-site-percolation model for various specimens prepared under the same conditions, but with different packing factor P. The connectivity is given by $K = \Delta\rho_g/\Delta\rho$, where $\Delta\rho$ and $\Delta\rho_g$ are the difference in the resistivity between 300 K and a temperature just above the critical temperature for a polycrystalline sample and for a high-quality single crystal, respectively. If the proportion of grain boundaries that are not covered with insulating oxide layers is

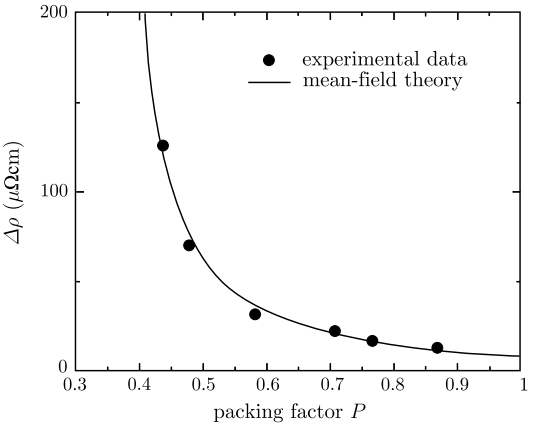

Fig. 9.4 Dependence of the difference in resistivity, $\Delta\rho$, between 300 K and a temperature just above the critical temperature, in polycrystalline MgB_2 bulk samples on the packing factor, P [4]. The *symbols* and *solid line* show experimental results and the theoretical predictions of the percolation model, respectively

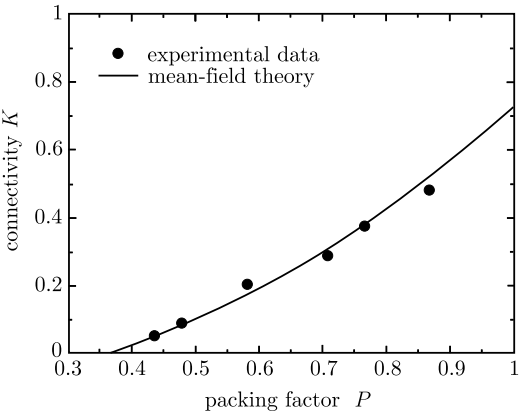

Fig. 9.5 Relationship between the connectivity, K, in polycrystalline MgB_2 bulk samples and the packing factor, P [4]. The *symbols* and *solid line* show experimental results and theoretical predictions from (9.1)

a, the connectivity is analytically given by

$$K = \frac{(aP)^2 - P_c^2}{1 - P_c^2}, \tag{9.1}$$

where $P_c = 0.3117$ is the threshold packing factor. In the analysis, $\Delta\rho_g$ and a were used as fitting parameters to obtain a good agreement between the experimental results and the theoretical analysis. From the comparison shown in Fig. 9.4, $\Delta\rho_g = 6.32\ \mu\Omega\,\mathrm{cm}$ and $a = 0.866$ were obtained [4]. The obtained value of $\Delta\rho_g$ was larger than the $4.3\ \mu\Omega\,\mathrm{cm}$ that Rowell used [3]. This is because the measured samples are randomly oriented polycrystals, while the value that Rowell used is the in-plane resistivity of a single crystal. The in-plane resistivity estimated using the bond-percolation model for a randomly oriented sample with full packing factor was $4.32\ \mu\Omega\,\mathrm{cm}$, which is quite similar to Rowell's value. This agreement suggests that the analysis by the percolation model describes the phenomena correctly.

Figure 9.5 shows the obtained relationship between the connectivity, K, and the packing factor, P. It shows that the connectivity of usual *in situ* wires with $P \simeq 0.5$

is only 10 % or so, and the reason for the low critical current densities is explained. Hence, it can be concluded that the packing factor should be increased to enhance the critical current density. In addition, it is also important to increase a, and improvement of the fabrication process is desired to suppress the formation of thin insulating oxide layers. For this purpose, it has been reported that removal of B_2O_3 by purification of B powders is effective [5]. In particular, the removal of adhesive B_2O_3 from the surface of B powders is important.

Various trials have been conducted to increase the packing factor of MgB_2 to improve the critical current density. It was reported [6] that application of hot pressing to an *in situ* wire was effective for enhancing the critical current density at low fields by reduction of voids in the superconducting region. Yamada et al. [7] achieved an especially high critical current density of 4.5×10^8 A m^{-2} at 4.2 K and 10 T with this process. On the other hand, the powder-in-closed-tube (PICT) process was proposed to produce bulk superconductors with a high volume fraction with the aid of a high vapor pressure of Mg, and a high critical current density was reported [8]. In addition, it was also reported that very high density MgB_2 could be synthesized by a diffusion process between an Fe-Mg alloy substrate and a B sheet [9]. Furthermore, a packing factor close to 100 % was achieved by a diffusion process for a mixture of commercial MgB_2 powder and B powder using the PICT method [10]. Recently, Hässler et al. [11] prepared a precursor material from Mg and B powders mixed with nanosize particles of C by using the mechanical alloying process and fabricated a tape by swaging a CuNi/Ni sheath filled with the precursor material, which was followed by a heat-treatment in Ar atmosphere at 625 °C for 3 hours. They obtained a high critical current density over 6×10^8 A m^{-2} at 4.2 K and 10 T. Addition of In or Sn was also proposed to fill voids in order to improve the connectivity among grains [12].

The *ex situ* process is better for achieving a higher packing factor of MgB_2. The connectivity in *ex situ* processed samples is lower, however, than that of *in situ* processed samples, as shown in Fig. 9.6 [13]. This gives us the reason why the critical current density in *ex situ* processed wires is low. The reaction to form the MgB_2 phase occurs in a process in which melted Mg diffuses into B powders, resulting in high connectivity between MgB_2 grains. Already formed MgB_2 grains in an *ex situ* superconductor do not connect tightly, however, even with a long heat-treatment at fairly high temperatures. The difference in the critical current density comes from the differences in the morphology of the MgB_2 grains and vacancies. That is, while MgB_2 grains in *in situ* wires envelope vacancies as in a porous material, maintaining current paths, wide and thin vacancies are likely to cover MgB_2 grains and restrict current paths in *ex situ* wires. As a result the connectivity among MgB_2 grains is not improved in *ex situ* wires, even when the packing factor increases [13].

The reason for such a structure of vacancies is considered to be the shrinkage of MgB_2 grains during self-sintering at high temperatures. Since vacancies disturb planar contacts between grains, the bond percolation model that focuses on the connectivity between sites seems to describe the phenomenon better as a percolation

approximation. The cubic-bond-percolation model predicts the connectivity as

$$K = \frac{aP - P_{bc}}{1 - P_{bc}}, \tag{9.2}$$

where $P_{bc} = 1/3$ is the threshold value. In this case, the connectivity changes linearly with the packing factor P, in comparison with (9.1). From comparison with the experimental results in Fig. 9.6, we obtain $a = 0.641$. Thus, the planar connectivity between grains in *ex situ* wires is inferior in comparison with that in *in situ* wires.

Various trials have been performed to overcome this weak point of the *ex situ* process. For example, the critical current density was improved by using MgB_2 powders prepared at 600 °C below the melting temperature [14], and the connectivity was increased to a comparable level to *in situ* wires by improving the uniformity of powders by introducing ball milling [15]. A reaction of unreacted Mg is speculated to increase the connectivity between grains in the former case, and oxide layers on the surface of the material powders might be broken by ball milling, resulting in the increase in the connectivity, in the latter case. It is important to further improve the critical current density through various investigations.

The packing factor appreciably influences the critical current density in MgB_2 superconductors, as discussed above. It should be noted that the high field property represented by the irreversibility field is also strongly influenced by the packing factor, as will be shown later. In fact, an enhancement of the irreversibility field was reported from increasing the packing factor by cold pressing [16]. The theoretical analysis of such behavior will be discussed in Sect. 9.3.2.

It is well known that addition of SiC is effective for improving the critical current density in MgB_2 wires. Figure 9.7 shows an example [17]. Added C atoms occupy B sites, and the honeycomb structure of the B atoms is distorted. As a result, the unit length of the a-axis is reduced by the addition, while that of the c-axis is not changed [18]. The improvement of the critical current density at high fields results from the improvement of the irreversibility field due to the enhanced upper critical

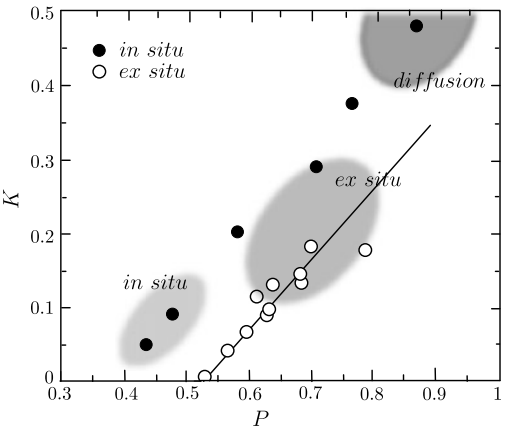

Fig. 9.6 Comparison of connectivity between *ex situ* samples (including a diffusion-processed sample) and *in situ* samples [13]. The *solid line* shows the theoretical predictions of (9.2) with $a = 0.641$

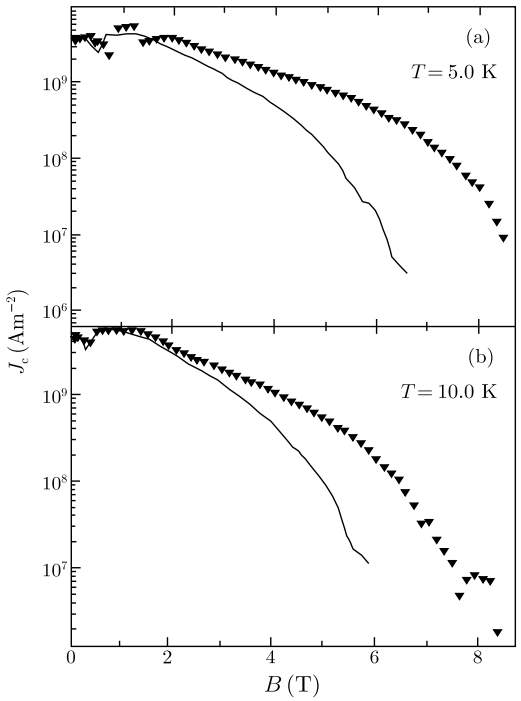

Fig. 9.7 Improvement of critical current density at (**a**) 5.0 K and (**b**) 10.0 K by addition of 10wt% fine SiC powders to MgB_2 [17]. *Solid symbols* show the results for the SiC-added specimen

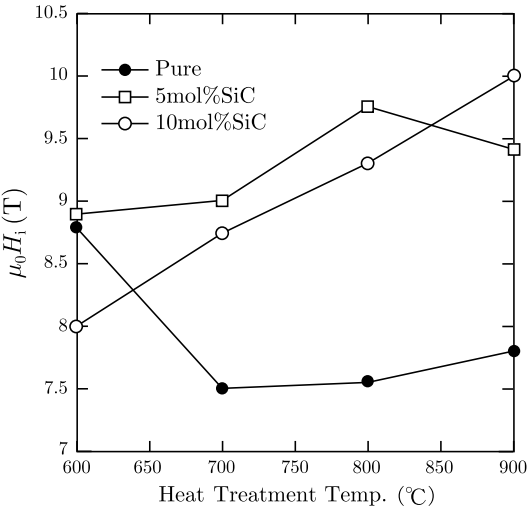

Fig. 9.8 Dependence of the irreversibility field at 20 K in MgB_2 specimens with different amounts of SiC addition on the temperature for the 1 h sintering [19]

field, which is brought about by reduction in the coherence length due to the distortion of the crystal structure by C substitution. Figure 9.8 shows the influence on the irreversibility field at 20 K of the amount of SiC addition and the temperature of a 1 h heat treatment [19]. For pure specimens, the irreversibility field is decreased

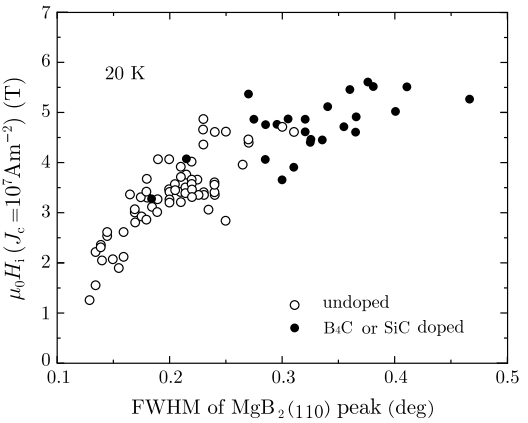

Fig. 9.9 Dependence of the irreversibility field on the FWHM of the (110) X ray diffraction peaks at 20 K for pure specimens and specimens doped with B_4C or SiC [20]

significantly by a heat treatment at high temperature. This can be attributed to the reduction in the upper critical field. On the other hand, the irreversibility field is likely to increase with the heat-treatment temperature in the SiC doped material. This is because the critical temperature is improved without reduction in the upper critical field by the sintering at high temperatures.

Figure 9.9 presents the relationship between the full-width at half-maximum (FWHM) of the (110) X ray diffraction peaks and the irreversibility field at 20 K for pure specimens and specimens doped with B_4C or SiC [20]. It shows that the irreversibility field increases with the FWHM. The crystal structure is deformed by the C addition, and the deformation causes the change in the pinning property. This change is ascribed partly to the enhancement of the upper critical field and may also be partly due to the enhancement of the flux pinning strength of grain boundaries by the electron scattering mechanism (see Sect. 6.3.2). The latter possibility will be clarified later by an analysis of experimental results.

Not only SiC addition, but also addition of carbon nanotubes [21], B_4C [22] or aromatic hydrocarbons [23] is effective for the improvement of the critical current properties at high magnetic fields. Among them, SiC is usually best, since the substitution rate at the B sites is highest for SiC. In the future, it will be necessary to seek the optimum amount of C substitution so that the impurity parameter takes a higher value than 1, in order to enhance the flux pinning strength of the grain boundaries.

Recently it has been found that the irreversibility field is also increased by synthesis at low temperatures such as 600 °C [24]. In fact, a relationship between the irreversibility field and the FWHM of XRD peaks, similar to that shown in Fig. 9.9, is obtained also for pure specimens synthesized at different temperatures [25], although the distortion which causes the increase in FWHM is not that of the honeycomb structure of B due to the C substitution, but the distortion due to fine grain structures. This fine grain structure is also expected to directly contribute to the improvement of the irreversibility field through the increase in the number density of pinning centers. The merit of the low temperature synthesis is that it does not cause deterioration of the critical temperature. Hence, this procedure is more advantageous than C-addition for applications at temperatures higher than 20 K.

Table 9.1 Specifications of specimens

Specimen	1	2	3	4
	MgB_2	MgB_2	$MgB_{1.5}(B_4C)_{0.1}$	$MgB_{1.8}(SiC)_{0.2}$
Heat treat.	950 °C × 12 h	600 °C × 24 h	850 °C × 3 h	850 °C × 3 h
T_c (K)	38.6	38.2	35.4	35.5

Here, the results of a quantitative investigation are shown for the effects of C-addition and low temperature synthesis on the flux pinning properties. Specimen 1 was C-free and was synthesized at 950 °C for 12 h. Specimen 2 was also C-free but was synthesized at 600 °C for 24 h. Specimens 3 and 4 were doped with SiC and

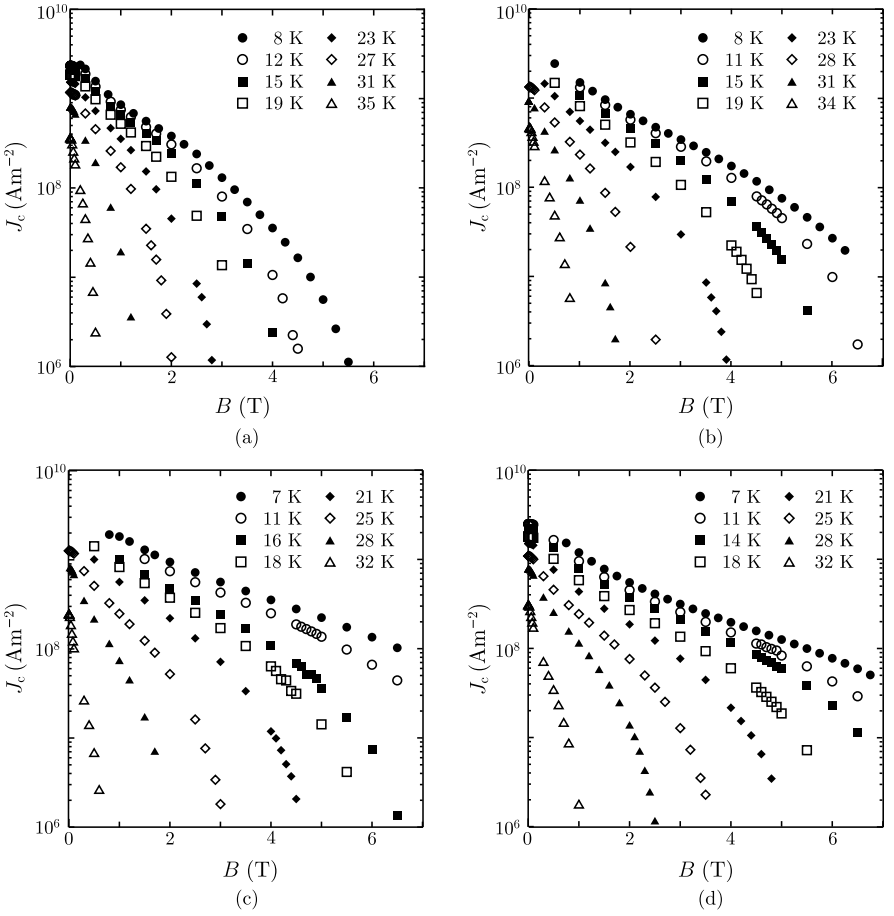

Fig. 9.10 Dependence of J_c of the individual MgB_2 specimens on magnetic field at various temperatures: (**a**) specimen 1, (**b**) specimen 2 synthesized at low temperature, (**c**) specimen 3 with B_4C addition, and (**d**) specimen 4 with SiC addition

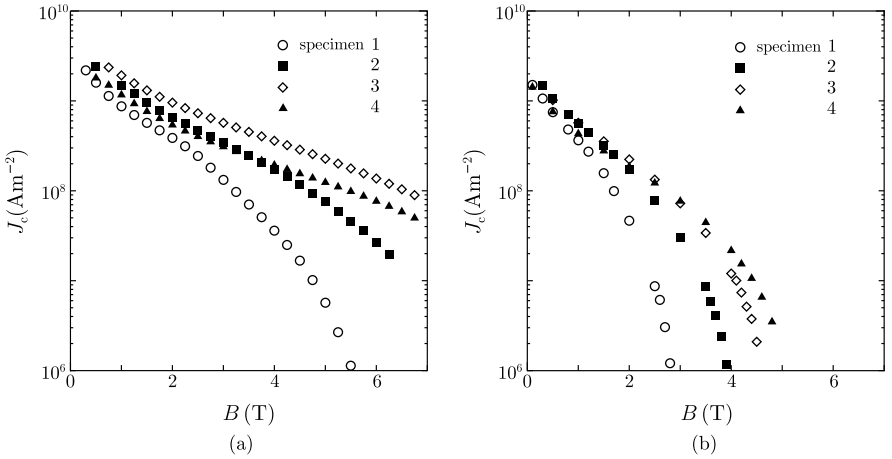

Fig. 9.11 Critical current density of each specimen at (**a**) $T/T_c = 0.2$ and (**b**) $T/T_c = 0.6$

B_4C, respectively, and were heat-treated at 850 °C for 3 h. These specimens were prepared by the PICT method. The specifications of the specimens are listed in Table 9.1. It can be seen that the critical temperature is above 38 K for pure specimens 1 and 2, and is degraded by about 3 K due to the C-addition. DC magnetization measurements were carried out on these specimens, and the critical current density was estimated. The obtained results are shown in Fig. 9.10. It was found that specimen 2 synthesized at low temperature has a considerably higher critical current density at low fields than specimen 1. On the other hand, the critical current density at high fields is significantly improved for specimens 3 and 4 with C-addition. Specimen 4 doped with B_4C shows a very high critical current density at low temperatures. The critical current densities of all the specimens at $T/T_c = 0.2$ and 0.6 are compared in Fig. 9.11 to clarify the characteristics of each specimen.

The scaling behavior of the pinning force density (F_p) of each specimen is shown in Fig. 9.12, where the solid line represents the relationship:

$$\frac{F_p}{F_{pmax}} \propto b_i^{1/2}(1 - b_i)^2, \tag{9.3}$$

where $b_i = B/\mu_0 H_i$ is the magnetic field normalized by the irreversibility field and F_{pmax} is the maximum pinning force density. The values of the irreversibility field at low temperatures were estimated from the extrapolation of the relationship of $(J_c B^{1-x})^{1/2}$ vs. B, which was linearized by adjusting the value of x. It was found that this relationship fits well with the results for specimen 1 over the entire range of measurement temperatures and with the results for the other specimens in the high temperature region. Note that the normalized magnetic field at which the pinning force density is at a maximum is appreciably smaller than 0.2, which is predicted by (9.3), suggesting a different pinning mechanism in the low temperature region for the three specimens other than specimen 1.

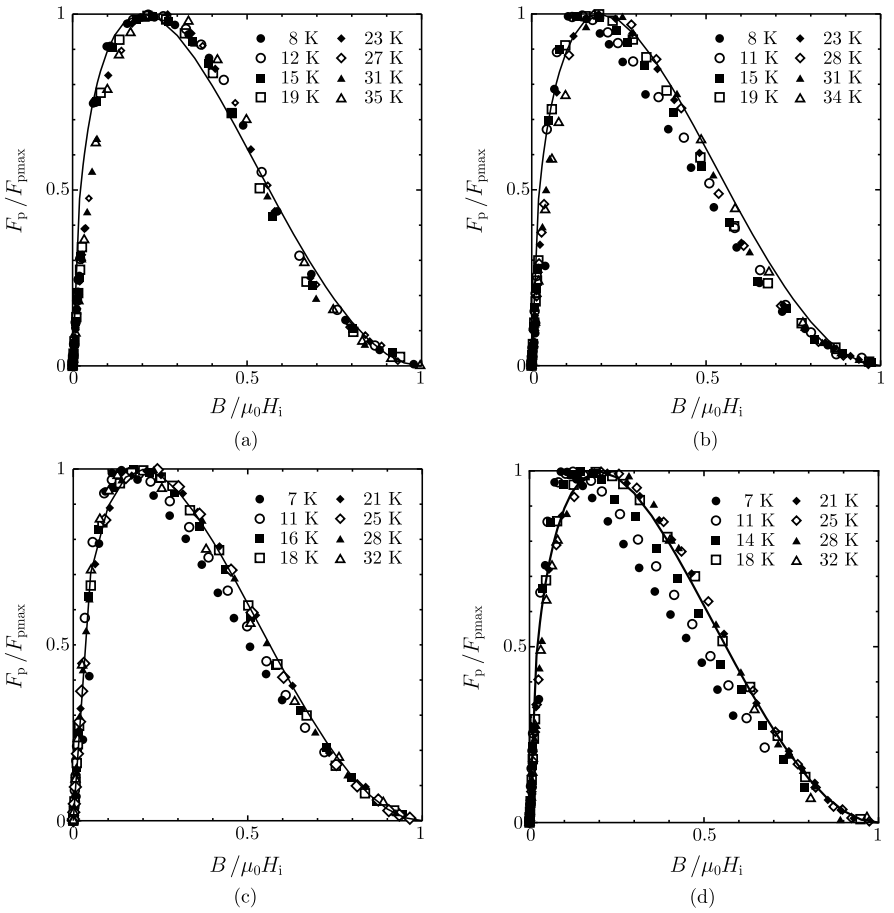

Fig. 9.12 Scaling law of the pinning force density of each MgB_2 specimen: (**a**) specimen 1, (**b**) specimen 2 synthesized at low temperature, (**c**) specimen 3 with B_4C addition, and (**d**) specimen 4 with SiC addition in Fig. 9.10. The *solid line* shows the scaling law of (9.3)

Figure 9.13 shows the temperature dependence of the irreversibility field for the four specimens. The irreversibility field is significantly enhanced in specimens 3 and 4 with C-addition and is considerably increased also in specimen 2, which was synthesized at low temperature. The critical current density in the high field region is accompanied by such an improvement in the irreversibility field. The temperature dependence of the irreversibility field is almost linear for all the specimens at high temperatures. At low temperatures, although the irreversibility field is somewhat saturated with decreasing temperature in the specimen synthesized at high temperature, it increases remarkably in the C-added specimens. The behavior of the specimen synthesized at low temperature is intermediate between them.

The relationship between F_{pmax} and H_i, i.e., the temperature dependence of the maximum pinning force density, is shown in Fig. 9.14. In the high temperature re-

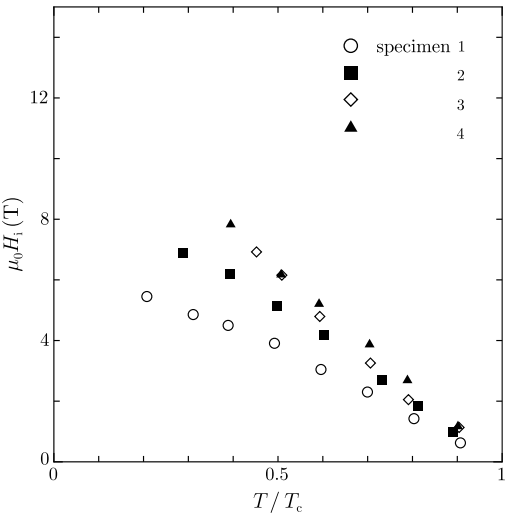

Fig. 9.13 Irreversibility field of each MgB_2 specimen as a function of the normalized temperature

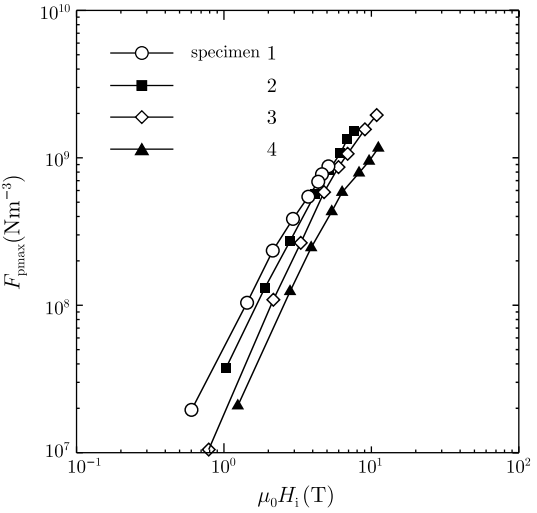

Fig. 9.14 Relationship between the maximum pinning force density and the irreversibility field. *Lines* are only guides for the eye

gion, F_{pmax} is proportional to the second power of H_i for all the specimens. On the other hand, the dependence of F_{pmax} on H_i is weaker at low temperatures, and this tendency is significant in the specimens with C-addition.

The shift of the maximum of the pinning force density to a low field in specimens 2–4 may be explained by a new contribution from point defects, etc. at low fields. If so, however, F_{pmax} must increase more in the low field region, resulting in a contradiction with the experiments shown in Fig. 9.14. If the slower rate of increase of F_{pmax} in the low temperature region is caused by weak links at grain boundaries, as in Y-123 superconductor, only the high critical current density at low fields would be limited, which would result in a shift of F_{pmax} to a higher field.

Another reason for the shift of F_{pmax} to a lower field may be an extraordinary increase in the irreversibility field at low fields, as indicated by the results in Fig. 9.13. When the superconductor becomes extremely dirty, the upper critical field is significantly enhanced at low temperatures because of the two gap superconductivity, resulting in the enhancement of the irreversibility field at low temperatures. On the other hand, the temperature dependence of the thermodynamic critical field, on which the flux pinning property directly depends, would not be so much different from that in fairly clean superconductors. Such a difference in the temperature dependence between the upper critical field and the thermodynamic critical field may be the reason for the change in the scaling behavior of the pinning force density at low temperatures.

9.2.2 Thin Films

There are mainly two methods for the fabrication of MgB_2 thin films: an indirect method in which magnesium is diffused into a deposited thin film by a heat-treatment and a direct method to fabricate the compound without heat-treatment. Using the former method, the critical temperature can be increased to a value comparable to those in bulk specimens or single crystals by a heat-treatment at high temperatures, although the upper critical field is not high. On the other hand, using the latter method, whereas the critical temperature is fairly low, the upper critical field can be significantly increased. Hence, the latter method is advantageous for applications at high fields. This is attributed to the short coherence length due to the electron scattering by the boundaries of fine grains in the thin film. The reduction in the critical temperature is also caused by the strain in the crystalline structure of the fine grains.

The upper critical field and irreversibility field parallel to the *c*-axis are shown in Fig. 9.15 for thin films fabricated by the two methods [26]. One of them is an *ex situ* thin film, which was fabricated by sealing a boron precursor film wrapped in Ta foil with Mg pellets and Ar gas in a stainless steel tube and then heat-treating it at 900 °C for 30 min, and the other is an *in situ* thin film, which was directly deposited from a MgB_2 target using the pulsed laser deposition technique and then heat-treated at 685 °C for 12 min. Although the critical temperature is higher, the enhancement of the upper critical field and irreversibility field with decreasing temperature is not significant for the former thin film. The enhancement of these fields in the latter thin film is significant.

The critical current density in thin films is generally higher than those in bulk specimens or wires. This is partly owing to the stronger flux pinning strength of grain boundaries at higher density due to the small size of grains, but the largest reason for the difference is a high packing factor close to 1. Such a high density of grain boundaries also contributes to the enhancement of the upper critical field. Nevertheless, the volume of flux bundles is limited because of the film thickness, resulting in a low irreversibility field under a strong influence of flux creep.

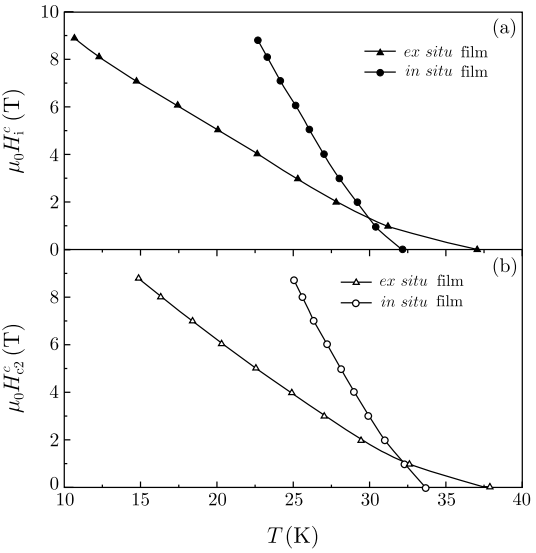

Fig. 9.15 Temperature dependence of the upper critical field and the irreversibility field parallel to the c-axis of the two kinds of MgB_2 thin film [26]

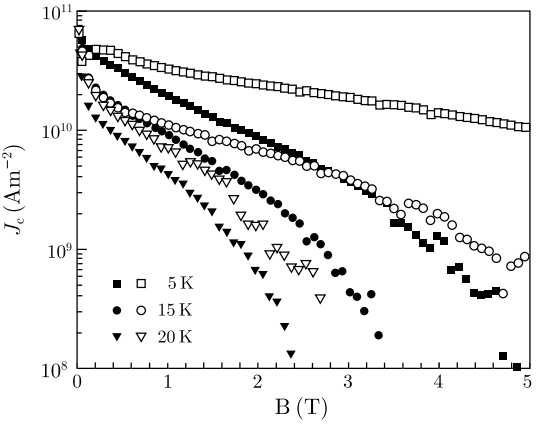

Fig. 9.16 Field dependence of the critical current density in a normal field for an *ex situ* thin film heat-treated at 900 °C (*solid symbols*) and an *in situ* thin film heat-treated at 650 °C (*open symbols*) [26], the upper critical field and irreversibility field of which are shown in Fig. 9.15

Figure 9.16 shows the critical current density for the two thin films prepared by the different methods [26], the upper critical fields of which have been shown in Fig. 9.15. The critical current densities of the two films at low fields are approximately the same and are very high. Hence, the flux pinning strength seems to be comparable in both. The value of the *ex situ* thin film annealed at high temperature is lower at high fields, however, due to the lower irreversibility field. This can be attributed to the lower value of the upper critical field. The high critical current density of 2.5×10^{11} A m^{-2} was attained for a similar *ex situ* thin film in self field at 5 K by Kwang et al. [27], although J_c quickly decreased with increasing field and was about 1×10^{10} A m^{-2} at 4.5 T. Such a difference in the magnetic field dependence of the critical current density between *ex situ* thin films made at high temperatures and *in situ* thin films made at low temperatures is fundamentally the same as the

difference between bulk specimens made at high temperatures and those made at low temperatures, which have been discussed in Sect. 9.2.1.

Zhuang et al. [28] fabricated an epitaxial thin film about 100 nm thick on a SiC substrate using a hybrid physical-chemical vapor deposition technique and obtained a very high critical current density of 8×10^{11} A m^{-2} in self-field at 2 K. They also reported an extremely high critical current density of 2.3×10^{12} A m^{-2} at 5 K and 0 T from a magnetization measurement in a normal magnetic field. The critical current density rapidly drops off with increasing magnetic field in a similar way to common thin films, and this can be attributed to the strong influence of flux creep because of the small flux bundle volume, which is limited by the film thickness.

9.3 Flux Pinning Properties

MgB_2 bulk is a polycrystalline compound superconductor, and its grain boundaries are known to act as pinning centers [29]. Figure 9.17 shows the relationship between the critical current density at 4.5 K and 5 T, and the reciprocal grain size [30]. The proportionality extending over a wide range proves the pinning interaction by the grain boundaries. The critical current density is only of the order of 1×10^8 A m^{-2}, however, even for the small grain size of $d_g = 0.2$ μm, which is 2–3 % of the critical current density of Nb_3Sn under the same conditions. This fact may suggest that the flux pinning strength of the grain boundaries is very weak in MgB_2. Such a low critical current density is attributed to the low connectivity caused by voids, however, as was discussed in Sect. 9.2.1.

In the following subsections, the elementary pinning force of grain boundaries in MgB_2 will be discussed, and then, it will be shown that the critical current density at low fields is simply determined by the connectivity, grain size, and elementary

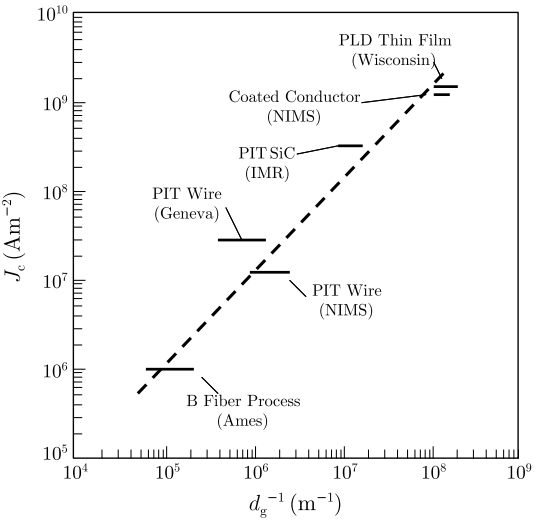

Fig. 9.17 Relationship between the critical current density at 4.2 K and 5 T, and the reciprocal grain size for MgB_2 superconductors [30]

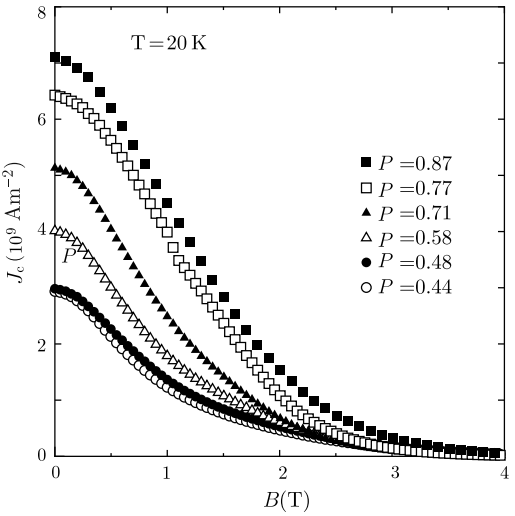

Fig. 9.18 Magnetic field dependence of the critical current density at 20 K for polycrystalline MgB_2 samples with different packing factors P [4]

pinning force of the grain boundaries. It will also be shown that the irreversibility field is influenced by the percolation property and flux creep, and that the pinning property changes in a complicated way at high fields.

9.3.1 Pinning Property in the Low Field Region

First, the critical current density at a low field ($b = B/\mu_0 H_{c2} = 0.1$) at 20 K is discussed. Since this field is sufficiently lower than the irreversibility field, the effect of flux creep is not taken into account. In addition, the anisotropy is neglected, and bulk superconductors are treated as equivalent isotropic superconductors for simplicity. The effect of the anisotropy is taken into account in the high field property in Sect. 9.3.2. The pinning mechanism of grain boundaries is the electron scattering by the grain boundaries, as discussed in Sect. 6.3.2. Since a quantitative analysis is only possible for specimens with known parameters such as the packing factor and connectivity, we analyze the pinning properties of the samples shown in Fig. 9.5. The magnetic field dependence of the critical current density of these samples at 20 K is shown in Fig. 9.18. The upper critical field, H_{c2}, is different from sample to sample, depending on the fabrication method, and Table 9.2 lists the parameters of the samples. It is necessary to describe correctly the elementary pinning force that depends on the impurity parameter. Hence, we cannot use the theoretical model of Zerweck [31], in which the inaccurate Goodman's interpolation formula is assumed. We use the theoretical model of Yetter et al. [32] based on the experimental results on Nb and follow the analysis in [33].

In the beginning, it is necessary to estimate the impurity parameter, α_i, defined in (6.24). For this purpose we have to estimate the BCS coherence length, ξ_0, of MgB_2. Then, the Ginzburg-Landau coherence length, ξ, at 20 K was determined

Table 9.2 Parameters of MgB_2 samples with different packing factors. The quantities P, K, α_i, $\hat{f}_{pn}$ and D_g are the packing factor, connectivity, impurity parameter, relative elementary pinning force, and effective grain size, respectively [33]

Sample	P	K	T_c [K]	$\mu_0 H_{c2}(20\ \mathrm{K})$ [T]	α_i	$\hat{f}_{pn}$	D_g [μm]
Bulk1	0.438	0.050	38.2	12.3	0.344	1.00	0.153
Bulk2	0.480	0.090	38.1	10.1	0.312	0.95	0.196
Bulk3	0.583	0.202	38.7	9.8	0.151	0.66	0.197
Bulk5	0.766	0.374	38.9	9.4	0.048	0.30	0.097

from the observed values of H_{c2}. On the other hand, the electron mean free path, l, can be determined from the correct value of the residual resistivity for samples with known connectivity. Here, the relationship between α_i and the coherence length at 0 K, $\xi(0)$, is approximated as

$$\xi(0) = \frac{0.67\xi_0}{(0.80 + \alpha_i^{0.80})^{0.37}}, \tag{9.4}$$

based on the results on Nb obtained by Yetter et al., and we can determine $\xi(20\ \mathrm{K})$ from $\xi(0)$, estimated from (6.24) and (9.4) with an assumed value of ξ_0. The value of ξ_0 can be determined in such a way that the values of $\xi(20\ \mathrm{K})$ obtained from the above two methods globally agree with each other for a series of samples. Using this method, $\xi_0 = 6.45$ nm was obtained [33]. The relationship between $\xi(0)/\xi_0$ and α_i is shown in Fig. 9.19. Open circles show the data for Nb obtained by Yetter et al., and the solid, dotted, and chained lines show the results from (9.4), the experimental formula by Yetter et al., and (6.27) by Welch [34], respectively. It can be seen that (9.4) expresses the behavior of Nb correctly. The behavior of MgB_2 is similar to that of Nb. The results in Fig. 9.18 clarify that the MgB_2 samples in Table 9.2 are not dirty superconductors.

Then, we will determine the elementary pinning force of grain boundaries at $b = 0.1$ in each sample. Only the value of the elementary pinning force in Nb was given, however, and the value of the condensation energy density was not described in [32]. Hence, their theoretical result cannot be directly applied to the MgB_2 samples. So, the elementary pinning forces in the samples were determined in such a way that the theoretical pinning force densities agree with the observed values [33]. We denote the elementary pinning force on a flux line of unit length parallel to a grain boundary by $\hat{f}_p$ and the elementary pinning force normalized by that in sample 1 by $\hat{f}_{pn}$. Table 9.2 shows these values for all the samples.

If we assume the direct summation model, the pinning force density in an ideal superconductor with the full connectivity ($K = 1$) at low magnetic fields is given by (7.83a), (7.83b). Taking account of the connectivity, K, the practical critical current density is

$$J_c = \frac{K\hat{f}_p}{D_g a_f B}, \tag{9.5}$$

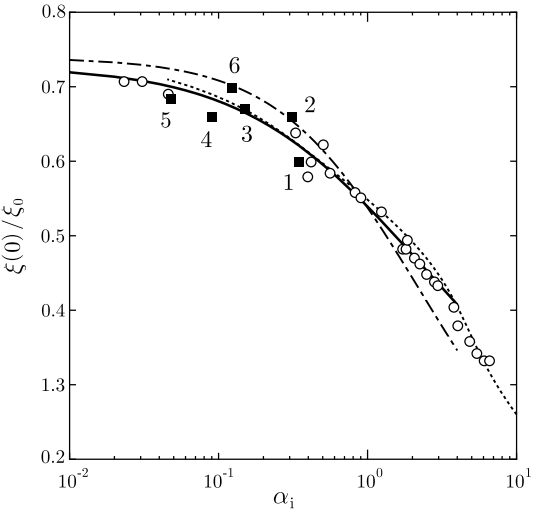

Fig. 9.19 Relationship between the ratio of coherence lengths $\xi(0)/\xi_0$ in MgB_2 and impurity parameter α_i shown by the *solid squares* [33]. *Open circles* are experimental data for Nb, and the *solid*, *dotted*, and *chained lines* show the results of (9.4), the experimental formula by Yetter et al. [32], and the formula by Welch [34], respectively. The numbers refer to the numbers of the samples in Table 9.2

where a_f is the flux line spacing and D_g is the effective grain size given by

$$D_g = \sum_{i=1}^{N} d_{gi}^3 \Big/ \sum_{i=1}^{N} d_{gi}^2 \tag{9.6}$$

with d_{gi} denoting the grain size of the i-th grain. Here, we denote the critical current density at $b = 0.1$ as

$$J_c(b = 0.1) = \frac{K C \hat{f}_{pn}}{D_g}, \tag{9.7}$$

where C represents a theoretical fitting parameter for the elementary pinning force of Yetter et al. That is, $C = (\hat{f}_p(\#1)/Ba_f)_{b=0.1}$ with $\hat{f}_p(\#1)$ denoting the elementary pinning force of Bulk1 sample. If we assume as $C = 0.330 \times 10^4$ A m^{-1}, (9.7) agrees well with the observed critical current density, as shown in Fig. 9.20.

The above results show that the critical current density at low magnetic field is determined by the flux pinning mechanism of the grain boundaries, and it can be concluded that the important factors are the connectivity, the pinning force of the grain boundaries, and the reciprocal grain size, which gives the effective number density of pinning centers, as predicted by (9.7).

Here, the above result is compared with the case of Nb_3Sn, in which the grain boundaries are similarly dominant pinning centers. The relationship between the maximum pinning force density at 4.2 K and the reciprocal grain size in Nb_3Sn was investigated by Scanlan et al. [35]. The flux pinning strength of grain boundaries in MgB_2 under the same conditions has been examined. It is assumed that an ideal condition of $K = 1$ is attained for the Bulk1 sample in Table 9.2 with the strongest elementary pinning force. The value of $\mu_0 H_{c2}$ in this sample at 20 K is 12.3 T, and hence, $b = 0.1$ corresponds to $B = 1.23$ T. Since the pinning force

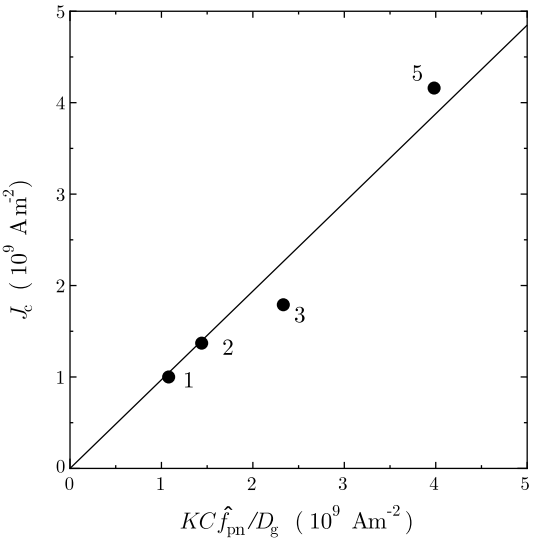

Fig. 9.20 Comparison of the critical current density at $b = 0.1$ and 20 K with the theoretical predictions of (9.7) shown by the *solid line* [33]. The numbers refer to the numbers of the samples in Table 9.2

density reaches its maximum at around this field at 20 K, it is convenient for comparison. The observed maximum pinning force density in the Bulk1 sample at 20 K is 1.2×10^9 N m^{-3}. Corrections for K and the difference in temperature between 4.2 and 20 K are necessary. As to the former correction, we have only to multiply by a factor of $1/K = 20$. When the temperature is reduced from 20 K to 4.2 K, the condensation energy density and the irreversibility field are expected to increase by factors of about 2.9 and 2.0, respectively. Then, the magnetic field at the maximum pinning force density is expected to increase by the same factor, 2.0, from the increase in the irreversibility field. If we remember that the pinning force density is proportional to $B^{1/2}$ from (9.5), since a_f is proportional to $B^{-1/2}$, the pinning force density is increased by a factor of $2.9 \times 2.0^{1/2} = 4.0$ by decreasing the temperature. Hence, it is expected that the ideal Bulk1 sample has the maximum pinning force density of 9.6×10^{10} N m^{-3}. On the other hand, when the relationship between the maximum pinning force density and the reciprocal grain size in Nb_3Sn is extrapolated to the fine grain size of 0.153 μm in the Bulk1 sample, the maximum pinning force density is estimated as 3.1×10^{10} N m^{-3}, which is about 1/3 of that in the Bulk1 sample [33]. This shows that the pinning force of grain boundaries in MgB_2 is very strong. This is partly ascribed to the fairly large impurity parameter of the Bulk1 sample. Even for the Bulk5 sample, with a weak pinning force, as it was fabricated at a relatively high temperature, the pinning property is comparable to that in Nb_3Sn. This tells us that very high critical current densities in MgB_2 thin films are reasonable.

Such a strong pinning in MgB_2 comes from the high condensation energy density that is associated with the pinning energy and a fairly long coherence length. The factor, $\mu_0 H_c^2 \xi$, which influences the flux pinning strength, is compared between MgB_2 and the commercial superconductors, Nb-Ti and Nb_3Sn, in Table 9.3. It can be seen that MgB_2 is superior to the other two superconductors. In particular, the

Table 9.3 Comparison of the values of $(\mu_0 H_c)^2 \xi$ among bulk MgB_2, Nb-Ti, and Nb_3Sn (the data on MgB_2 are from [2])

	MgB_2		Nb-Ti	Nb_3Sn
	10 K	20 K	4.2 K	4.2 K
$\mu_0 H_c$ (T)	0.48	0.27	0.20	0.50
ξ (nm)	6.04	6.81	5.70	3.90
$(\mu_0 H_c)^2 \xi$ (T^2nm)	1.39	0.50	0.23	0.98

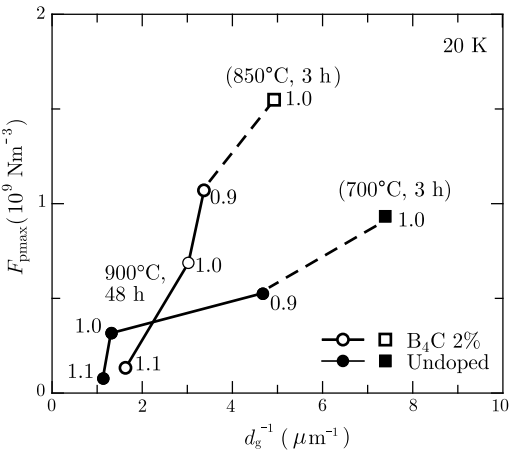

Fig. 9.21 Relationship between the maximum pinning force density and the reciprocal grain size for MgB_2 samples doped with 2 % B_4C and a non-doped samples [36]

superiority remains even at 20 K, if it is compared with Nb-Ti at 4.2 K. The pinning centers in Nb-Ti are not grain boundaries, however, but strong normal precipitates with a higher performance, and there is room for strengthening the flux pinning in MgB_2. Addition of C is effective for this purpose. The addition of C makes the coherence length shorter by scattering electrons, as shown in Fig. 9.7, and an increase in the elementary pinning force of grain boundaries can be expected, since MgB_2 is a relatively clean superconductor, as shown in Fig. 9.19. Hence, it is possible to remarkably increase the elementary pinning force by making the material dirty. In fact, Katsura et al. [36] showed that the elementary pinning force of grain boundaries can be increased by the addition of B_4C, as shown in Fig. 9.21. It is expected that the optimization of the elementary pinning force will be examined in detail.

9.3.2 Pinning Properties in the High Magnetic Field Region

The pinning properties in the high magnetic field region are influenced by the percolation property in a more complicated manner than in the low field region. For example, the irreversibility field varies with the packing factor, as shown in Sect. 9.2.1. MgB_2 is polycrystalline, and each grain has anisotropy with respect to the magnetic field direction. That is, the upper critical field and the irreversibility field are low for a grain with the *c*-axis close to the applied magnetic field direction, and this grain

ceases to transport the superconducting current at a relatively low magnetic field. Since such a grain is equivalent to a vacancy, the effective packing factor is reduced with increasing magnetic field. In a superconductor with a low packing factor, the effective packing factor reaches this threshold at a relatively low magnetic field, resulting in zero critical current density: this is the reason why the irreversibility field is low in a superconductor with a low packing factor. It is necessary to use a percolation model in which the anisotropy of randomly oriented grains is taken into account to analyze the pinning property in the high field region. In addition, it is also necessary to use the flux creep theory to treat the irreversibility field. Here, the theoretical treatment in [37], in which these points are considered, is briefly introduced.

First, the effect of flux-creep is considered to find out the density of the practical meandering current, and then, the percolation property is calculated. Finally, the effect of the distributed grain size is taken into consideration, since the sites must be equivalent to each other in the site-percolation model.

The flux pinning strength in the high field region must be considered. Here, the saturation type pinning property, discussed in Sect. 7.4, is assumed, since MgB_2 is a high κ superconductor. The virtual critical current density in the flux-creep-free case obeys

$$J_{c0} = AB^{-1/2}\left(1 - \frac{B}{\mu_0 H_{c2}}\right)^2, \tag{9.8}$$

where A is given by

$$A = \left(\frac{\sqrt{3}}{2\phi_0}\right)^{1/2} \frac{\hat{f}_p}{d_g}. \tag{9.9}$$

Since the distributed grain size is assumed, we do not use the effective grain size, D_g. If the angle of the c-axis of each grain from the direction of the applied field is θ, the upper critical field is

$$H_{c2}(\theta) = \frac{H_{c2}^c}{(\cos^2\theta + \gamma_a^{-2}\sin^2\theta)^{1/2}}, \tag{9.10}$$

where H_{c2}^c is the upper critical field along the c-axis and γ_a is the anisotropy parameter. The temperature at which the resistance starts to decrease in the resistance vs. temperature transition curve in a magnetic field is the temperature at which the applied field is equal to the maximum upper critical field, i.e., that in the a-b plane, $H_{c2}^{ab} = \gamma_a H_{c2}^c$. Thus, the characteristic transition curve, the upper critical field in the a-b plane vs. temperature, is obtained from the experimental results, and H_{c2}^c at 20 K was determined with $\gamma_a = 4.0$ around this temperature. Next, the critical current density in a grain with the c-axis tilted by θ from the magnetic field is numerically estimated using the flux creep and flow model in Sect. 8.5.2, in which the pinning potential, U_0, in the three-dimensional pinning is calculated with the above J_{c0}. The result is well approximated in the scaled form:

$$J_c(\theta) = DH_i^p(\theta)B^{\gamma-1}\left[1 - \frac{B}{\mu_0 H_i(\theta)}\right]^\delta. \tag{9.11}$$

As a result, the numerically fitted parameters are $p = 0.505$, $\gamma = 0.5$, and $\delta = 1.9$ for the Bulk1 sample with $d_g = 0.153$ μm. The irreversibility field, $H_i(\theta)$ is also determined numerically. The obtained values of γ and δ are close to the values assumed in (9.8), i.e., $1/2$ and 2, respectively. The anisotropy of the irreversibility field can be approximated in a similar form to (9.10):

$$H_i(\theta) = \frac{H_i(0)}{[\cos^2\theta + (\gamma_a')^{-2}\sin^2\theta]^{1/2}}, \tag{9.12}$$

where γ_a' is the apparent anisotropy parameter and is 3.92 in this case. That is, γ_a' is slightly smaller than γ_a.

Second, the effect of the percolation property is considered. In a superconductor, the critical current density of each grain is different because of the difference in the irreversibility field depending on the direction of the c-axis with respect to the direction of the field. That is, the irreversibility field is lower in a grain with the c-axis closer to the field direction, resulting in a smaller critical current density. We consider the situation where the superconducting current of density J flows in magnetic flux density B. Grains that can transport this current are those for which the critical current densities are higher than J. If the angle of the c-axis of a grain that has the critical current density just equal to J is denoted by θ_c, it can be determined by the condition:

$$J = DH_i^p(\theta_c)B^{\gamma-1}\left[1 - \frac{B}{\mu_0 H_i(\theta_c)}\right]^{\delta}. \tag{9.13}$$

Hence, the grains that can transport the superconducting current with density J are those with a crystal angle θ larger than θ_c. If the fraction of such grains is denoted by $P_e(B, J)$, it is given by

$$P_e(B, J) = \frac{aP}{2\pi}\int_0^{2\pi} d\phi \int_{\theta_c}^{2\pi} \sin\theta d\theta = aP\cos\theta_c, \tag{9.14}$$

where ϕ is the azimuthal angle in the plane normal to the applied magnetic field. Hence,

$$K(J) = \frac{P_e^2(B, J) - P_c^2}{1 - P_c^2} \tag{9.15}$$

gives the proportion of grains that can transport the superconducting current with a density higher than J. The local critical current density under a magnetic flux density B is determined by the direction of the magnetic field, and the minimum and maximum values are respectively given by

$$\begin{aligned} J_{cm} &= DH_i^p(0)B^{\gamma-1}\left[1 - \frac{B}{\mu_0 H_i(0)}\right]^{\delta}; \quad B < \mu_0 H_i(0), \\ &= 0; \quad B > \mu_0 H_i(0), \end{aligned} \tag{9.16}$$

and

$$J_{\mathrm{cM}} = DH_{\mathrm{i}}^{p}(\pi/2)B^{\gamma-1}\left[1-\frac{B}{\mu_0 H_{\mathrm{i}}(\pi/2)}\right]^{\delta}. \tag{9.17}$$

If all grains transport current with the same density J_{cm}, the average current density is

$$\langle J\rangle = J_{\mathrm{cm}}K(J_{\mathrm{cm}}). \tag{9.18}$$

When the current density is increased by ΔJ, the increase in the average current density is $\Delta J K(J_{\mathrm{cm}}+\Delta J)$. When the current density is further increased by ΔJ, the additional increase in the average current density is $\Delta J K(J_{\mathrm{cm}}+2\Delta J)$. As a result, the average current density reaches finally

$$\langle J\rangle = J_{\mathrm{cm}}K(J_{\mathrm{cm}}) + \int_{J_{\mathrm{cm}}}^{J'_{\mathrm{cM}}} K(J)\mathrm{d}J, \tag{9.19}$$

where J'_{cM} is the substantial maximum current density determined by the condition:

$$K\left(J'_{\mathrm{cM}}\right) = 0. \tag{9.20}$$

After a numerical calculation, the average pinning force density is approximately expressed as

$$\langle F\rangle = \langle J\rangle B = GB^{\gamma'}\left(1-\frac{B}{\mu_0 H_{\mathrm{ie}}}\right)^{\delta'}, \tag{9.21}$$

where G, γ', H_{ie}, and δ' are numerically determined parameters. The results for the Bulk1 sample are shown in Fig. 9.22 [37]. The solid symbols are numerically calculated results, and the solid line represents (9.21) with $\gamma' = 0.52$, $\delta' = 2.10$, and $\mu_0 H_{\mathrm{ie}} = 4.0$ T.

Finally, the effect of the distributed grain size is considered. It should be noted that the irreversibility field H_{ie} is proportional to $G^{1/3}$, as shown in (8.40) because of the proportionality of G in (9.21) to the inverse of the grain size. The calculated results on the Bulk1 sample based on the observed grain size distribution are shown in Fig. 9.23 and compared with the experimental results [37]. Although the theoretical irreversibility field is slightly lower than the observations, a relatively good agreement is obtained. The reason for the lower theoretical irreversibility field may be found in the possibility of underestimation of the upper critical field when observed resistively because of the flux creep. The analyzed maximum pinning force density and irreversibility field for the four samples in Table 9.2 are compared with the experimental results in Figs. 9.24 and 9.25 [37]. Since the irreversibility field depends largely on the upper critical field, the ratio with respect to the upper critical field is shown. In addition, the effect of the elementary pinning force is also compensated by introducing the factor of $\hat{f}_{\mathrm{pn}}^{1/3}$. Thus, it can be concluded that the maximum pinning force density and the irreversibility field depend strongly on the

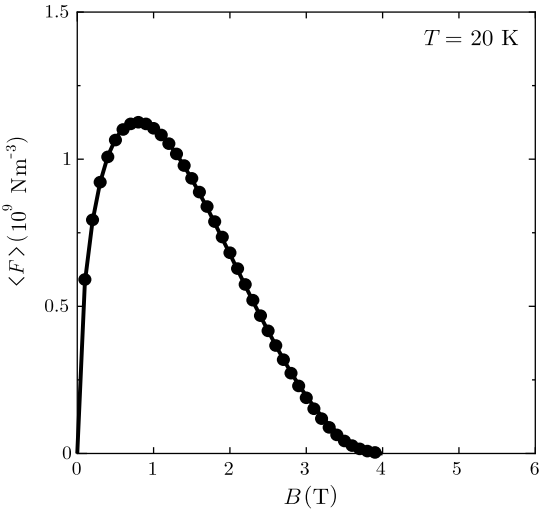

Fig. 9.22 Magnetic field dependence of the average pinning force density at 20 K in the Bulk1 sample with $d_g = 0.153$ μm [37]. *Solid symbols* are the numerically calculated results, and the *solid line* represents (9.21) with $\gamma' = 0.52$, $\delta' = 2.10$, and $\mu_0 H_{ie} = 4.0$ T

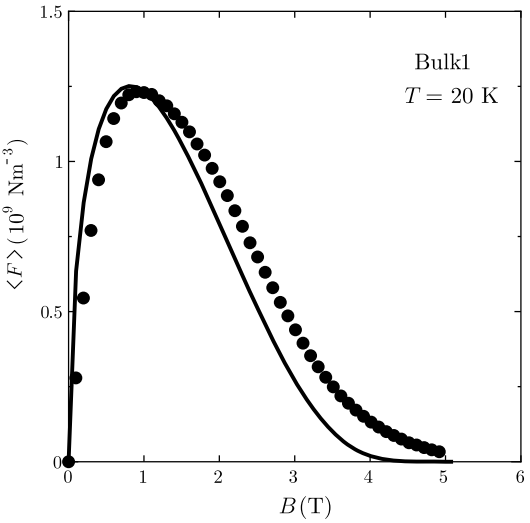

Fig. 9.23 Magnetic field dependence of the pinning force density of the Bulk1 sample at 20 K [37]. *Solid symbols* are experimental results and the *solid line* shows the theoretical results

packing factor. Increasing the packing factor is important for improvement of the high-field properties.

In comparison with randomly oriented bulk MgB_2 superconductors, the crystals are well aligned in thin films, and this causes a large anisotropy of the irreversibility field. In particular, the irreversibility field parallel to the c-axis is fairly low, resulting in a rapid decrease in the critical current density of a thin film with increasing field in the normal direction, as shown in Fig. 9.16. This deterioration with field originates from the flux creep and also from a low value of the upper critical field. Such weak points are compensated by averaging in randomly oriented wires and bulks.

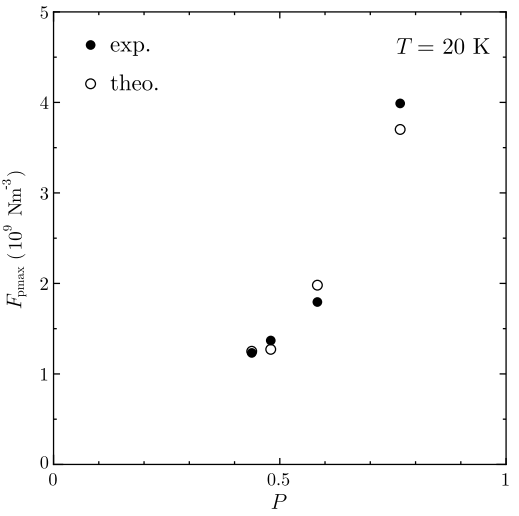

Fig. 9.24 Packing factor dependence of the maximum pinning force density [37]. *Solid* and *open symbols* are experimental and theoretical results, respectively

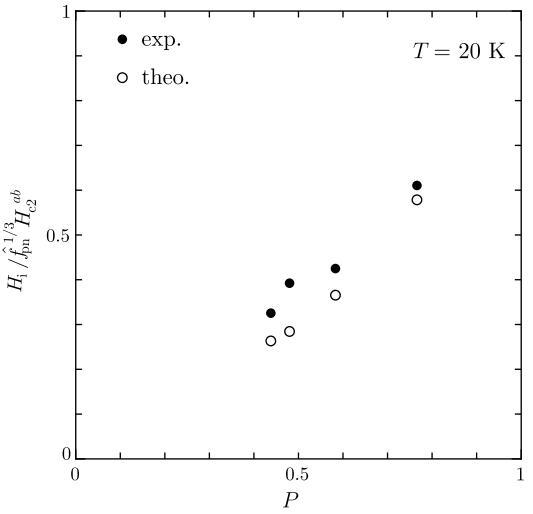

Fig. 9.25 Packing factor dependence of the irreversibility field normalized by the upper critical field [37]. The effect of the elementary pinning force is compensated. *Solid* and *open symbols* are experimental and theoretical results, respectively

9.4 Exercises

9.1 Assume that the impurity parameter, α_{i}, is increased to 0.750 by addition of C to a bulk MgB_2 superconductor. Estimate the average value of $\mu_0 H_{\mathrm{c2}}$ at 0 K.

9.2 Assume that the packing factor P and effective grain size D_{g} in the bulk superconductor in Exercise 9.1 are 0.70 and 100 nm, respectively. Estimate the critical current density at 20 K and 1 T. It is assumed that $a = 0.866$ and that the critical temperature is the same as that of the Bulk1 sample in Table 9.2, 38.2 K. The relative elementary pinning force for $\alpha_{\mathrm{i}} = 0.750$ is $\hat{f}_{\mathrm{pn}} = 1.32$.

9.3 Determine the critical current density at 4.2 K and in a normal magnetic field of 1 T for a MgB_2 thin film with full connectivity ($K = 1$). Assume that the effective grain size D_g in this field direction is 0.050 μm and that the impurity parameter α_i is 0.151, which is the same as for the Bulk3 sample in Table 9.2. The critical temperature T_c is 38.2 K, and (1.2) is assumed for the temperature dependence of the thermodynamic critical field, $H_c(T)$.

References

1. L. Lyard, P. Samuely, P. Szabo, T. Klein, C. Marcenat, L. Paulius, K.H.P. Kim, C.U. Jung, H.-S. Lee, B. Kang, S. Choi, S.-I. Lee, J. Marcus, S. Blanchard, A.G.M. Jansen, U. Welp, G. Karapetrov, W.K. Kwok, Phys. Rev. B **66**, 180502 (2002)
2. M. Fukuda, E.S. Otabe, T. Matsushita, Physica C **378–381**, 239 (2002)
3. J.M. Rowell, Supercond. Sci. Technol. **16**, R17 (2003)
4. A. Yamamoto, J. Shimoyama, K. Kishio, T. Matsushita, Supercond. Sci. Technol. **20**, 658 (2007)
5. J. Jiang, B.J. Senkowicz, D.C. Larbalestier, E.E. Hellstrom, Supercond. Sci. Technol. **19**, L33 (2006)
6. Y. Yamada, M. Nakatsuka, K. Tachikawa, H. Kumakura, Teion Kōgaku **40**, 493 (2005)
7. H. Yamada, M. Igarashi, Y. Nemoto, Y. Yamada, K. Tachikawa, H. Kitaguchi, A. Matsumoto, H. Kumakura, Supercond. Sci. Technol. **23**, 045030 (2010)
8. A. Yamamoto, J. Shimoyama, S. Ueda, Y. Katsura, S. Horii, K. Kishio, Supercond. Sci. Technol. **17**, 921 (2004)
9. K. Togano, T. Nakane, H. Fujii, H. Takeya, H. Kumakura, Supercond. Sci. Technol. **19**, L17 (2006)
10. I. Iwayama, S. Ueda, A. Yamamoto, Y. Katsura, J. Shimoyama, S. Horii, K. Kishio, Physica C **460–462**, 581 (2007)
11. W. Hässler, M. Herrmann, C. Rodig, M. Schubert, K. Nenkov, B. Holzapfel, Supercond. Sci. Technol. **21**, 062001 (2008)
12. K. Tachikawa, Y. Yamada, M. Enomoto, M. Aodai, H. Kumakura, Physica C **392–396**, 1030 (2003)
13. A. Yamamoto, H. Tanaka, J. Shimoyama, H. Ogino, K. Kishio, T. Matsushita, Jpn. J. Appl. Phys. **51**, 010105 (2012)
14. H. Tanaka, A. Yamamoto, H. Ogino, J. Shimoyama, K. Kishio, Abstracts of CSSJ Conf., vol. 84 (2011) p. 43 [in Japanese]
15. H. Tanaka, A. Yamamoto, J. Shimoyama, H. Ogino, K. Kishio, Supercond. Sci. Technol. **25**, 115022 (2012)
16. R. Flükiger, M.S.A. Hossain, C. Senatore, Supercond. Sci. Technol. **22**, 247002 (2009)
17. S.X. Dou, A.V. Pan, S. Zhou, M. Ionescu, H.K. Liu, P.R. Munroe, Supercond. Sci. Technol. **15**, 1587 (2002)
18. H. Yamada, M. Hirakawa, H. Kumakura, H. Kitaguchi, Supercond. Sci. Technol. **19**, 175 (2006)
19. H. Kumakura, H. Kitaguchi, A. Matsumoto, H. Yamada, Supercond. Sci. Technol. **18**, 1042 (2005)
20. A. Yamamoto, J. Shimoyama, S. Ueda, Y. Katsura, I. Iwayama, S. Horii, K. Kishio, Appl. Phys. Lett. **86**, 212502 (2005)
21. W.K. Yeoh, J.H. Kim, J. Horvat, S.X. Dou, P. Munroe, Supercond. Sci. Technol. **19**, L5 (2006)
22. A. Yamamoto, J. Shimoyama, S. Ueda, I. Iwayama, S. Horii, K. Kishio, Supercond. Sci. Technol. **18**, 1323 (2005)
23. H. Yamada, M. Hirakawa, H. Kumakura, H. Kitaguchi, Supercond. Sci. Technol. **19**, 175 (2006)

24. A. Yamamoto, J. Shimoyama, S. Ueda, Y. Katsura, S. Horii, K. Kishio, Supercond. Sci. Technol. **18**, 116 (2005)
25. A. Yamamoto, J. Shimoyama, M. Ueda, I. Iwata, Y. Katsura, S. Horii, K. Kishio, Teion Kōgaku **40**, 466 (2005)
26. Y. Zhao, M. Ionescu, J. Horvat, S.X. Dou, Supercond. Sci. Technol. **17**, S482 (2004)
27. W.N. Kang, E.M. Choi, H.J. Kim, H.J. Kim, S.I. Lee, Physica C **385**, 24 (2003)
28. C.G. Zhuang, S. Meng, C.Y. Zhang, Q.R. Feng, Z.Z. Gan, H. Yang, Y. Jia, H.H. Wen, X.X. Xi, J. Appl. Phys. **104**, 013924 (2008)
29. H. Kitaguchi, A. Matsumoto, H. Kumakura, T. Doi, H. Yamamoto, K. Saitoh, H. Sosiati, S. Hata, Appl. Phys. Lett. **85**, 2842 (2004)
30. K. Togano, private communication
31. G. Zerweck, J. Low Temp. Phys. **42**, 1 (1981)
32. W.E. Yetter, D.A. Thomas, E.J. Kramer, Philos. Mag. B **46**, 523 (1982)
33. T. Matsushita, M. Kiuchi, A. Yamamoto, J. Shimoyama, K. Kishio, Supercond. Sci. Technol. **21**, 015008 (2008)
34. D.O. Welch, IEEE Trans. Magn. **MAG-21**, 827 (1985)
35. R.M. Scanlan, W.A. Fietz, E.F. Koch, J. Appl. Phys. **46**, 2244 (1975)
36. Y. Katsura, A. Yamamoto, I. Iwayama, S. Ueda, J. Shimoyama, S. Horii, K. Kishio, J. Phys. Conf. Ser. **43**, 119 (2005)
37. T. Matsushita, J. Tanigawa, M. Kiuchi, A. Yamamoto, J. Shimoyama, K. Kishio, Jpn. J. Appl. Phys. **51**, 123103 (2012)